Effect of firing temperature on humidity self-regulation functionality in a ceramic tile composition

J. Castellano, V. Sanz, E. Cañas, E. Sánchez

Instituto de Tecnología Cerámica (ITC), Universitat Jaume I (UJI), Castellón, Spain

Javier Castellano* Telephone number: (+34) 964342424
Email: javier.castellano@itc.uji.es

Vicente Sanz
Email: sanzs@uji.es

Eugeni Cañas
Email: eugeni.canas@itc.uji.es

Enrique Sánchez
Email: enrique.sanchez@itc.uji.es

Abstract

The effect of sintering temperature on the humidity regulating capacity of a ceramic composition based on the mineral gibbsite has been studied. The humidity self-regulation functionality is due to the presence of mesopores in the material.

In this work, it has been found that the adsorption-desorption capacity decreases drastically with sintering temperature, preserving a certain regulating activity up to temperatures as high as 1200 ºC. The variation of the regulating capacity with temperature is consistent with the transformation of gibbsite from transition alumina to alpha alumina, which leads to a sharp decrease of the mesopore volume which can be determined from mercury porosimetry and especially nitrogen gas adsorption.

The adsorption-desorption curves fit well to a pseudo-second order kinetic model and it is found that the equilibrium moisture is proportional to the specific surface area while the sorption rate constant depends on permeability for water diffusion through the porous structure.

Keywords: moisture adsorption, mesopores, kinetic model, gibbsite, firing temperature.

1 Introduction

The development of construction materials that contribute to reduce the energy consumption of buildings is a subject of undoubted interest in society. Indoor air conditioning in buildings, both private and public, by using air conditioners is a common practice that has experienced a remarkable growth in recent years, especially in countries with warmer climates, such as southern European countries. In this way, the electricity bill of buildings has increased dramatically in recent years and this growth is expected to continue in the coming years. Expectations for the growth of electricity consumption for cooling predict that this consumption will be dominant in buildings by 2050, with a cumulative growth of more than 750 %. In addition, this increase in electricity consumption is accompanied by a growth of CO_2 emissions [1-3].

It is therefore not surprising that the scientific community has taken an interest in the development of materials that can reduce, or eventually eliminate, the use of air conditioners. One of the strategies developed is to design porous ceramic materials with

the functionality of self-regulating humidity, in such a way that they can maintain the humidity of the room in the range of human comfort, between 40 and 70 % [4,5]. However, incorporating the functionality of humidity regulation in a ceramic tile that must be processed by heat treatment at high temperature is not easy. This is because the materials with humidity regulating capacity are characterised by a porous microstructure with a large volume of mesopores which develop the adsorption and desorption phenomena that regulate environmental humidity, as described in the literature [6,7]. When these materials are heat-treated, the porous nanostructure (mesoporosity) tends to collapse by pore coalescence, leading to an increase in pore size which results in a deterioration, and eventually a loss, of the humidity regulating capacity [8,9].

A review of the literature shows the use of natural raw materials, such as allophane, for the development of humidity regulating ceramic tiles [10,11]. Allophane can maintain its mesoporous structure up to temperatures of around 900 ºC, however, above that temperature the humidity regulating capacity is considerably reduced [12]. Moreover, being a rock of volcanic origin, its availability for the manufacture of ceramic tiles is very limited. Although other more common raw materials such as zeolite, bentonite, sepiolite and diatomite have been tested for incorporation in ceramic tiles, their active porous structure is only preserved at low temperatures (< 1000 ºC), well below those usually used in the industry for the manufacture of ceramic tiles [13-16]. In another work, Vu et al. have managed to reach higher temperatures up to 1100 °C while preserving the adsorption-desorption capacity, but the composition is mainly based in diatomite (90 %) giving rise to extremely high porous pieces that are very difficult to handle in a tile manufacturing process and which could not be marketed afterwards [17]. Recently, the authors of the present work have published an article where a kinetic study of the moisture adsorption and desorption capacity of ceramic tiles obtained from different ceramic compositions based on the mineral gibbsite has been carried out [18]. Excellent moisture regulation capacities have been obtained at temperatures above 1100 ºC, although the study was limited to a maximum temperature of 1120 ºC.

As indicated, the collapse of the mesoporous structure with increasing firing temperature is assumed to be the cause of the loss of humidity regulating capacity. Watanabe et al. even correlates the moisture adsorption capacity with the volume of mesopores (pore size between 2-50 nm), although, as mentioned above, the specimens were fired below 1000

ºC [10]. In addition, the incorporation of temperature in kinetic studies has hardly taken place and, above all, no attempt has been made to correlate the firing temperature with kinetic models of moisture adsorption-desorption capability.

As a consequence of the above, this work addresses to continue the previous research in order to evaluate the effect of the firing temperature on the humidity regulating capacity of ceramic tiles and to determine the maximum firing temperature at which this functionality can be preserved. For this purpose, the kinetic model developed in the previous work [18] will be used in order to correlate the parameters of the model with the firing temperature as well as the latter with the evolution of the porous structure of the fired pieces.

2 Experimental procedure

2.1 Materials and sample preparation

For the development of this work, an industrial composition already used in the first part of the study has been employed. This composition is used in industry for the manufacture of porous ceramics and is based on a mixture of gibbsite, white plastic clay and other minerals (talc and quartz) as reported [18]. It is an industrial composition, in the form of spray-dried powder, which showed an excellent humidity regulating capacity of interest for tile manufacturing.

Table 1 shows the chemical analysis of this powder obtained by wavelength dispersive X-ray fluorescence spectrometry (XRF; Axios, Panalytical). A Rh anode tube, 4 kW of working power and certified reference materials were used. The analysis was performed on beads of fused material, using a mixture of lithium tetraborate and lithium metaborate as a flux.

Mineralogical analysis of the powder by X-ray diffraction (XRD; D8 Advance diffractometer, Bruker Theta-theta) is shown in Table 2, indicating the amount of each phase in semi-quantitative form with asterisks. Cu Kα radiation at 40 kV and 30 mA was used for XRD analysis, with a range from $2\theta = 5^{\circ}$ until $2\theta = 90^{\circ}$, a step size of 0.02° and a scanning speed of 0.5 $s \cdot step^{-1}$.

Regarding particle size, the specific surface area of the powder is 7.7 m^2/g (BET method) and the mean particle size is 18.5 μm (laser diffraction).

Table 1. Chemical analysis (in wt%) for the studied composition [18]

SiO_2	Al_2O_3	Fe_2O_3	CaO	MgO	Na_2O	K_2O	Others	LOI
32.9	38.9	0.4	0.5	5.7	0.4	0.3	0.3	20.6

Table 2. Mineralogical analysis with identified phases for the studied composition (asterisks denote a semi-quantitative amount)

Identified phase	Quantity
Gibbsite ($Al(OH)_3$)	***
Talc ($Mg_3Si_4O_{10}(OH)_2$)	**
Kaolinite ($Al_2Si_2O_5(OH)_4$)	**
Quartz (SiO_2)	**
Illite / Muscovite ($KAl_3Si_3O_{10}(OH)_2$)	*
Dolomite ($CaMg(CO_3)_2$)	*

The spray-dried powder was conditioned by wetting it to a moisture content of 5.5 % on a dry basis and pressed at 300 $kg \cdot cm^{-2}$. All the pressed bodies were fully dried in a laboratory oven at 110 ºC. Subsequently, the pressed specimens were fired in a laboratory electric furnace (RHF 1400, Carbolite) following a firing cycle with a heating rate of 5 $ºC \cdot min^{-1}$ and a dwell time at maximum temperature of 6 minutes. The maximum firing temperatures were chosen to range from 1050 to 1250 ºC with an increment of 50 ºC, which covers by far the usual firing temperatures of ceramic tiles in industrial practice.

2.2 Samples characterisation

Firing diagram was built by determining linear shrinkage and water absorption of the bodies fired at the different maximum firing temperatures. Linear shrinkage was calculated dimensionally from the difference between the dry and fired diameters of the specimens measured with a calliper, defining this parameter on a dry basis. Water absorption was determined by the boiling method, measuring the weight gain experienced by the specimens when placed in boiling water for a period of 2 h. The microstructures at different temperatures were characterised by examining the fractured cross section with a field-emission gun environmental scanning electron microscope (FEG-ESEM; Quanta 200 FEG, FEI Company). The samples for FEG-ESEM were platinum coated by

sputtering before inspection and the secondary electron detector signal under high vacuum conditions was used during the observation, taking micrographs at 2500x and 40000x magnifications. Additionally, crystalline phase evolution with temperature in fired specimens was analysed by XRD.

Humidity regulating capacity was assessed by adsorption and desorption tests carried out in a climatic chamber (HC2020, Heraeus Vötsch). This chamber allows regulating the temperature and relative humidity conditions, keeping the temperature constant during the whole test and modifying the relative humidity according to convenience. An adsorption-desorption cycle was carried out as follows. The specimens were placed inside the chamber, the temperature was set at 23 ºC and the relative humidity at 50 % for sufficient time to reach equilibrium with a minimum time of 16 h. The initial weight of the pieces (m_0) was determined, reintroduced into the chamber increasing the relative humidity to 90 % and weighing was performed at increasing time periods (m_t) for 24 h or until equilibrium was reached (80 h). The incremental amount of water adsorbed for each time (q_t) was calculated as a percentage from Eq. (1). Moisture desorption was then determined in an analogous way by varying the relative humidity from 90 % to 50 % and performing the corresponding weighing.

$$q_t(\%) = \frac{m_t - m_0}{m_0} \cdot 100 \qquad \text{Eq. (1)}$$

The determination of pore size distributions was also carried out by mercury intrusion porosimetry and nitrogen gas adsorption. As previously mentioned [18], although the presence or absence of mesopores can be evidenced by mercury porosimetry, nitrogen adsorption is key for the characterisation since it allows determining specific surface area, total volume of mesopores and mean pore diameter. For the former, an automated mercury porosimeter (AutoPore IV 9500, Micromeritics) was used. The instrument measures the variation in the volume of mercury intrusion as a function of the applied pressure and it transforms the pressures into pore diameter values considering a mercury-ceramic contact angle of 130º. Before testing, the samples were dried at 110 °C.

Nitrogen adsorption/desorption curves were determined with a gas adsorption analyser equipment (TriStar 3000, Micromeritics) according to ISO 9277:2010. Prior to testing, the samples were dried and subjected to nitrogen stream degassing at 150 °C for 2 h. The specific surface area was calculated according to BET (Brunauer-Emmett-Teller) method

by multipoint determination. Pore volume and pore size distribution were calculated from the curves according to BJH (Barrett-Joyner-Halenda) method.

3 Results and discussion

3.1 Characterisation and firing behaviour of specimens

Figure 1 shows the variation of linear shrinkage and water absorption of dried specimens following the firing cycle set out above. As can be seen in the figure, the variation followed by both physical characteristics corresponds to the densification experienced by the composition through a sintering process. Indeed, as would be expected from the initial chemical and mineralogical composition, in which a mixture of refractory oxides (silica and alumina) coexists with minor oxides with a marked fluxing character (sodium or potassium oxides), the specimens undergo a gradual increase of linear shrinkage with temperature and a parallel decrease in porosity, because of the sintering process in the presence of liquid phase [19,20]. The presence of gibbsite as one of the main phases in the starting composition causes the water absorption of the product to remain at still high values (over 15 %) at temperatures at which the different types of ceramic tiles are usually fired (1160-1200 ºC). It is therefore a type of ceramic composition that would preserve a high porosity in the industrial firing cycles of tile manufacturing.

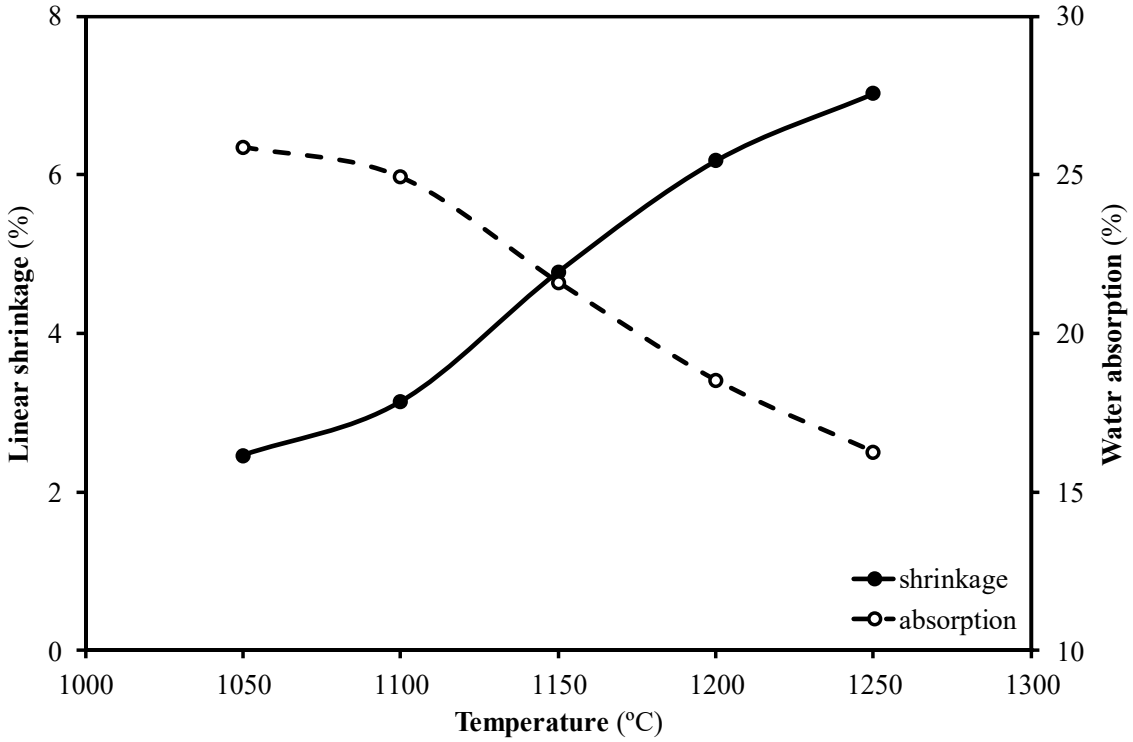

Figure 1. Firing diagram: linear shrinkage and water absorption variation with sintering temperature

Figure 2 shows the images taken with the FEG-ESEM microscope at two magnifications for the samples fired at 1050, 1150 and 1250 ºC. The micrographs reveal microstructural changes developed during the sintering process. As can be seen, the microstructure is formed by agglomerates of fine alumina platelets (marked with arrows) that contain smaller pores (mesopores) according to the micrographs in the bottom row, which detail the internal aspect of these agglomerates at higher magnification. A microstructure feature of amorphous transition alumina prevails at temperatures up to 1150 °C, but the crystallisation of alpha alumina (corundum) takes place at higher temperatures [21,22], being very evident in the images for the sample fired at 1250 ºC. This transformation leads to a significant increase in particle size with a collapse of the inner mesoporosity characteristic of transition alumina. Thus, non-crystalline transition alumina, which is present at lower temperatures, is responsible of a hierarchical porous structure containing the smallest pores of the fired specimen.

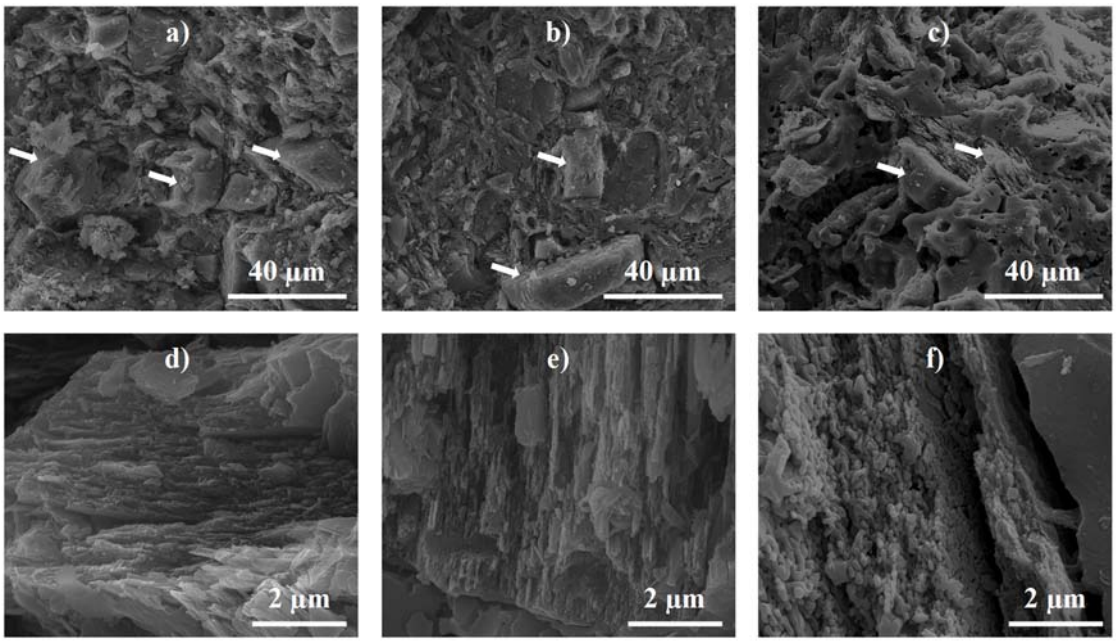

Figure 2. SEM micrographs of the samples fired at different temperatures: a) 1050 ºC, b) 1150 ºC and c) 1250 ºC. Interior detail of alumina agglomerates at higher magnification: d) 1050 ºC, e) 1150 ºC and f) 1250 ºC

Evolution of crystalline phases with sintering temperature was followed by X-ray diffraction. Figure 3 shows this evolution, indicating the appearance, the increase and the decrease of the main crystalline phases. According to the diffractograms in Figure 3, the appearance of alpha alumina (corundum) is evident from 1150 ºC and its presence increases with temperature. As reported in literature [21-23], alpha alumina is the last thermodynamically stable conversion formed from the transition aluminas when gibbsite is fired in cycles such as those carried out. Thus, gibbsite follows a transformation sequence with temperature, firstly into transition aluminas (mainly chi at low temperature and kappa at higher temperature) and finally into alpha alumina (corundum). These findings agree with the microstructural changes in Figure 2 and the collapse of the mesoporous structure in favour of coarser pores associated with the crystallisation of alpha alumina. At higher temperatures, the appearance of cristobalite and cordierite is observed together with a decrease in the intensity of the unreacted quartz peaks. This is characteristic of ceramic products with talc or other raw materials incorporating magnesia when sintered at high temperatures [24].

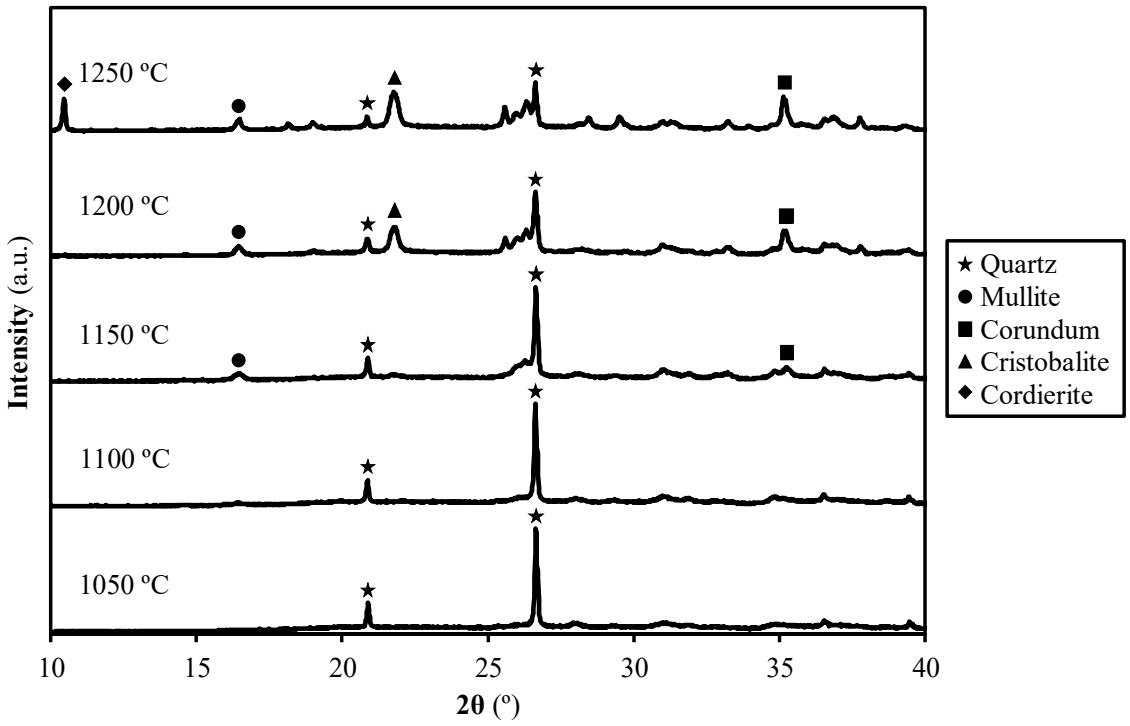

Figure 3. Evolution of main crystalline phases with sintering temperature

3.2 Evolution of humidity regulation capability with temperature

Figure 4 shows the moisture adsorption and desorption curves of the pieces at a constant temperature of 23 ºC in 24-h cycles. In the same figure, adsorption tests carried out at longer times (80 h) are also presented trying to reach equilibrium moisture plateau. For all temperatures it is observed that moisture desorption occurs at a faster rate than adsorption. Thus, most of the water vapour is released in the first eight hours whereas the whole process is completed in less than 24 h. On the contrary, although a significant amount of water is also adsorbed during the first hours of the test, the process continues after 24 h, with more modest variations, that follow an asymptotic trend up to the equilibrium value. The shape of the curves and the kinetic differences between adsorption and desorption are in line with the findings of other researches that have analysed water vapour adsorption and desorption phenomena from mesoporous materials [17,25,26].

On the other hand, a clear effect of sintering temperature on the amount of adsorbed water is observed. As the sintering temperature increases, the amount of adsorbed water decreases significantly and is drastically reduced at the highest sintering temperature tested (1250 ºC). Thus, for the lowest sintering temperature of 1050 ºC, the amounts of

adsorbed water at 24 h and 80 h were around 4 % and 6 % respectively, and for the temperature of 1250 ºC, both values were reduced down to 0.3 % and 0.5 % respectively. For comparison purpose, Figure 4a also shows the curves corresponding to an industrial composition of porous ceramic wall tiles, which has no moisture regulating capacity, as described in the previous work [18]. It can be observed that the moisture regulating capacity practically disappears at the maximum sintering temperature, resembling the industrial wall tile composition that lacks this functionality.

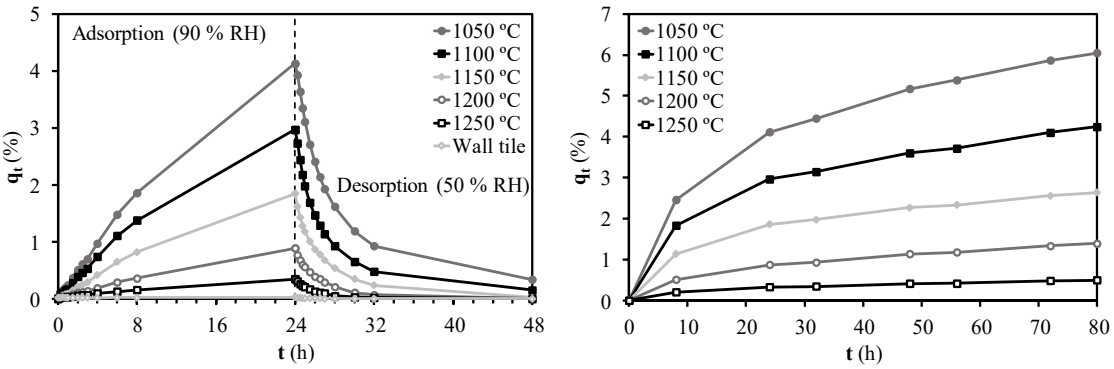

Figure 4. a) Adsorption-desorption curves for the samples sintered at different temperatures and b) Adsorption curves carried out at longer times (80 h). For comparison purpose the adsorption-desorption curves for an industrial composition of porous ceramic wall tiles, which has no moisture regulating capacity, is included

A kinetic analysis can be performed on the basis of the adsorption and desorption model successfully tested in the previous paper from the pseudo-second order equation of Lagergren [18]. The model equations were Eq. (2) for adsorption process and Eq. (3) for desorption process:

$$\frac{t}{q_t} = \frac{1}{Kq_e^2} + \frac{1}{q_e}t \qquad \text{Eq. (2)}$$

$$\frac{t}{q_0 - q_t} = \frac{1}{K(q_e - q_0)^2} + \frac{1}{q_e - q_0}t \qquad \text{Eq. (3)}$$

where q_e is the incremental amount of moisture at equilibrium, q_t is the incremental moisture at time t, q_0 is the incremental moisture at the beginning of desorption and K is the pseudo-second order sorption rate constant. Eq. (2) implies a linear relationship of the term t/q_t versus t for adsorption while Eq. (3) denotes a linear relationship between the

term $t/(q_0-q_t)$ and t for desorption. The parameters q_e and K can be calculated from slopes and ordinates at the origin of the graphs respectively.

The graphical representation of the fitting results for the adsorption isotherms at 80 h and desorption isotherms is shown in Figure 5. The goodness of fit to the pseudo-second order kinetic model can be seen in these graphs. Since the slope correlates inversely with equilibrium moisture content, the lines are ordered according to humidity regulation from lowest to highest, i.e., the steeper lines correspond to the samples with lower moisture regulation while the more horizontal lines belong to the samples with higher moisture regulation capacity.

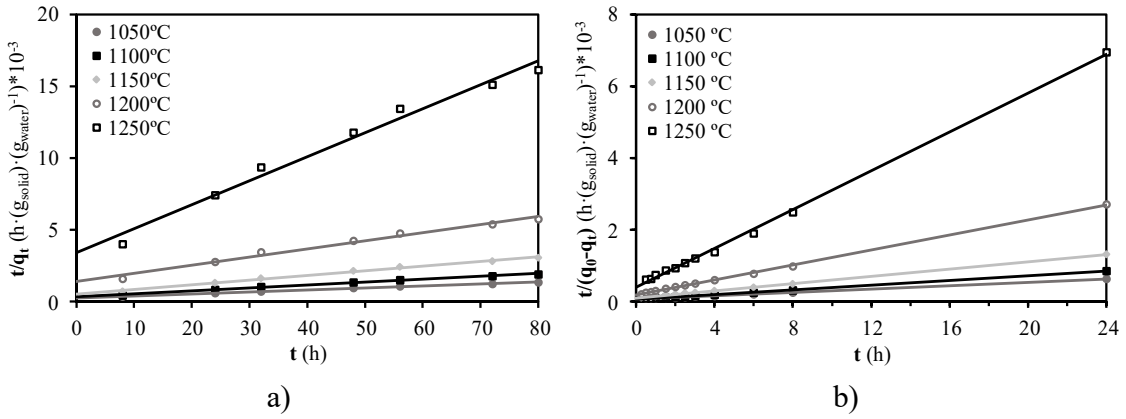

Figure 5. Fitting of a) adsorption curves for 80 h and b) desorption curves for 24 h to the pseudo-second order kinetic model

The kinetic parameters calculated from the slopes and ordinates at origin are detailed in Table 3. The proper fit of the results is corroborated by correlation coefficients close to unity. Moreover, similarity between equilibrium moistures for adsorption and desorption processes also confirm the consistency of the proposed model. The differences in kinetics between adsorption and desorption are revealed by observing the lower rate constants for adsorption compared to desorption.

Table 3. Kinetic parameters q_e and K and correlation coefficients obtained from the model fit for 80 h-adsorption and desorption experiments

T (ºC)	Adsorption (RH = 90 %)			Desorption (RH = 50 %)		
	K $(g\cdot(h\cdot g)^{-1})$	q_e (%)	R^2	K $(g\cdot(h\cdot g)^{-1})$	q_e (%)	R^2
1050	0.74 ± 0.09	7.3 ± 0.2	0.995	7.4 ± 0.5	8.45 ± 0.08	0.998
1100	1.2 ± 0.2	5.0 ± 0.2	0.993	14.6 ± 0.9	6.07 ± 0.05	0.998
1150	2.0 ± 0.3	3.1 ± 0.1	0.994	25.6 ± 0.7	3.83 ± 0.02	1.000
1200	2.3 ± 0.4	1.8 ± 0.1	0.984	58 ± 3	1.84 ± 0.02	0.999
1250	8.1 ± 0.9	0.60 ± 0.04	0.983	181 ± 9	0.72 ± 0.01	0.998

When analysing the results of the model fit, the effect of the sintering temperature on the moisture adsorption and desorption capacity of the pieces is evident. As the temperature augments, humidity regulation capacity strongly decreases as shown by the reduction in equilibrium moisture content. Thus, equilibrium moisture content diminishes approximately linearly from over 7 % down to 0.6 % as corresponding to a non-functional tile (porous ceramic wall tile). Overall, desorption experiments show similar values which in turn present the same variation degree with temperature. On the contrary, the parameter K exponentially increases with temperature for both processes whereas the values of this parameter considerably differ between adsorption and desorption. The fact that the sorption rate constant K increases with growing temperature probably relates to the lower number of pores to be filled as well as the enhanced accessibility of such porosity as the sintering process evolves with temperature. As extensively reported in literature [27,28], microstructure evolution with temperature leads to a pore coarsening effect which results in an enhancement of body permeability and accessibility of water vapour when the total porosity remains approximately constant or decreases slightly. Finally, for a given temperature (same piece microstructure) much higher K values in desorption denote a favourable evaporation or water vapour migration into the environment in comparison with capillary condensation. Hu et al. [26] have already reported kinetic differences between adsorption and desorption processes for diatomite humidity control materials, while other authors have noted the influence of pore diameter on the sorption and the role of H_2O–aluminosilicate and H_2O–H_2O interactions on the desorption rate [29]. A weaker H_2O–H_2O interaction, due to the adsorption of water on previously adsorbed water

molecules, compared to the interaction between water and material, due to the initial adsorption of water on the surface functional groups to form a first layer, could justify the higher desorption rate.

3.3 Analysis of mesoporosity and pore size distribution with temperature

The cumulative pore size distributions for the different samples from the mercury porosimetry analysis are presented in Figure 6. The characteristic values of the distributions, including total pore volume and percentage of open porosity, are detailed in Table 4. The pore size distributions highlight the differences of samples microstructures with temperature. At the lowest temperature (1050 ºC) the sample contains an appreciable amount of small pore sizes (mesopores) with diameters below 0.05 μm (50 nm) that provide the ability to regulate humidity to the material as reported elsewhere [6,7]. This mesoporosity reservoir decreases as the temperature grows being visible till 1200 ºC and practically disappearing at the highest sintering temperature of 1250 ºC. Data showed in Table 4 confirm the appreciation of Figure 6, the pore size increases with temperature while the pore volume and the porosity decrease due to higher sintering degree [30,31].

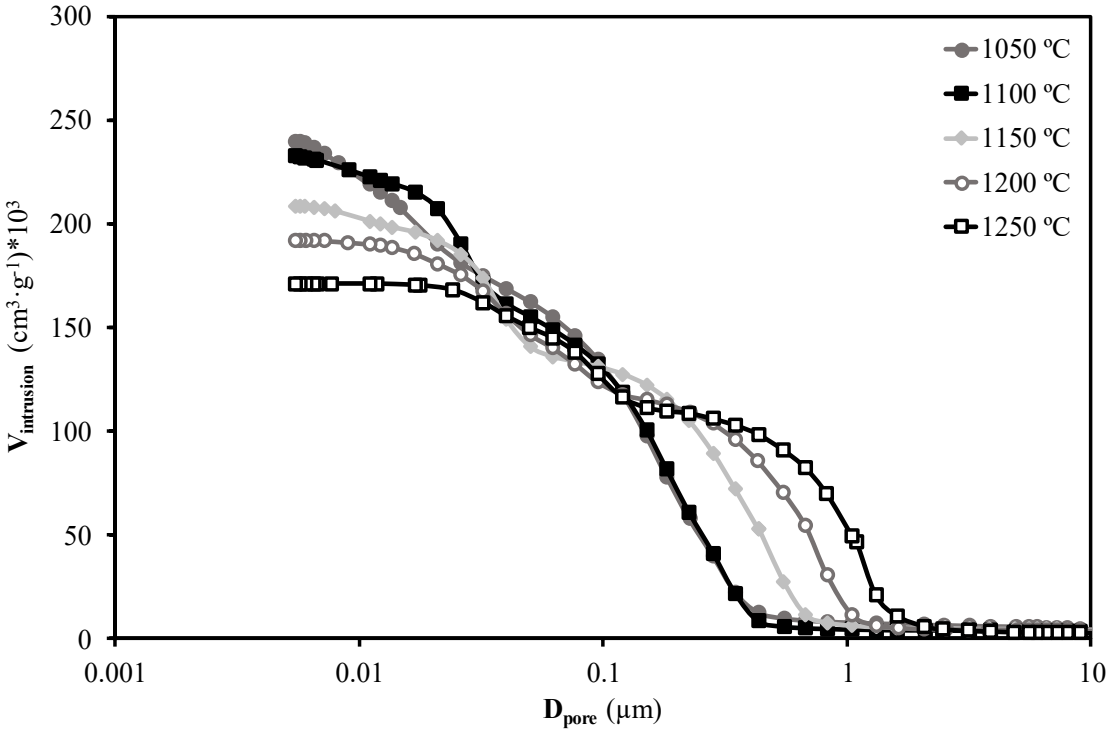

Figure 6. Cumulative pore diameter distributions by mercury porosimetry

Table 4. Characteristic values of pore size distribution (d_{16}, d_{50} and d_{84}), total pore volume (V_p) and percentage of open porosity (P) obtained by mercury porosimetry

T (ºC)	d_{16} (µm)	d_{50} (µm)	d_{84} (µm)	V_p ($cm^3 \cdot g^{-1}$)	P (%)
1050	0.29 ± 0.02	0.12 ± 0.01	0.02 ± 0.01	0.240 ± 0.005	40 ± 2
1100	0.30 ± 0.02	0.12 ± 0.01	0.02 ± 0.01	0.233 ± 0.005	39 ± 2
1150	0.52 ± 0.03	0.23 ± 0.02	0.03 ± 0.01	0.208 ± 0.005	37 ± 2
1200	0.83 ± 0.04	0.35 ± 0.02	0.04 ± 0.01	0.192 ± 0.005	35 ± 2
1250	1.26 ± 0.05	0.63 ± 0.03	0.07 ± 0.01	0.171 ± 0.005	33 ± 2

The nitrogen adsorption/desorption curves for all samples are shown in Figure 7. The curves display hysteresis according to a Type IV sorption behaviour, typical of materials with mesopores that are filled and emptied by capillary condensation [32]. The volume of nitrogen adsorbed follows the expected evolution dictated by the porosimetry curves, i.e. a clear decreasing with sintering temperature.

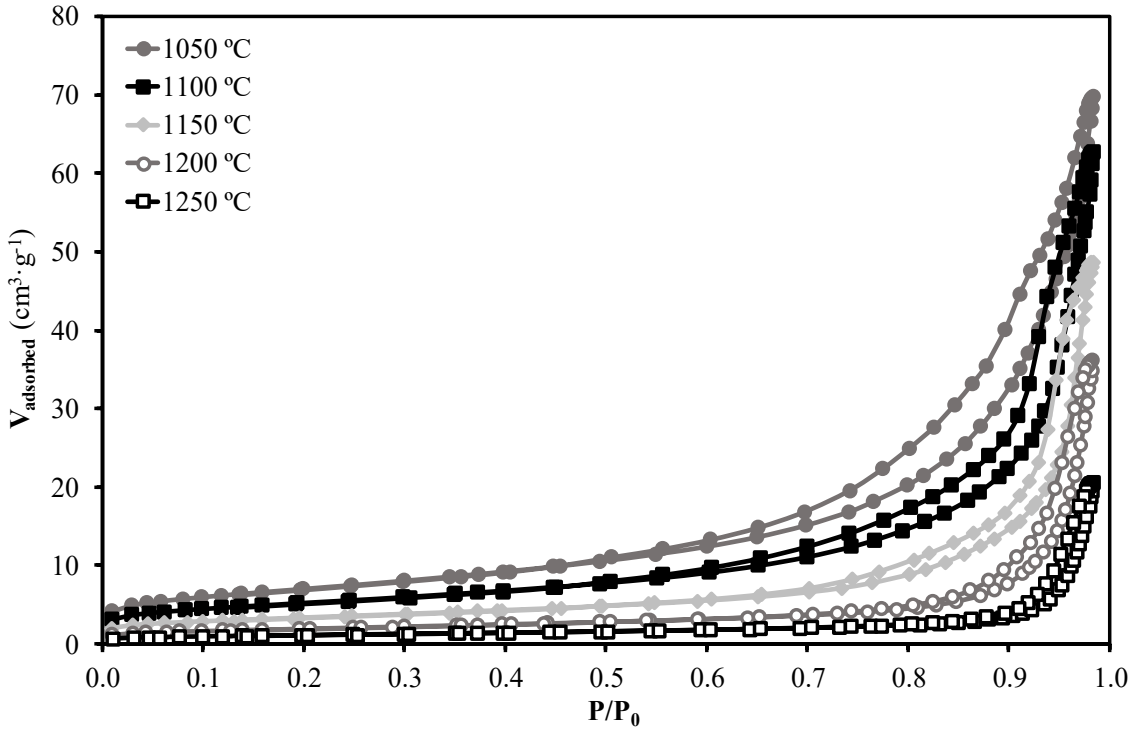

Figure 7. Nitrogen adsorption/desorption isotherms for all samples

The specific surface area can be easily determined from the adsorption/desorption curves according to BET method as detailed in Table 5 while the pore size distributions obtained according to BJH method are presented in Figure 8. Table 5 also shows the accumulated pore volume under desorption and the average pore diameter value, calculated as 4V/A where V is the volume and A is the total pore area. As observed, the results confirm the microstructure evolution determined by mercury porosimetry: as the sintering temperature rises the specific surface area strongly decreases leading to pore size distributions characterised by lower pore volume and higher mean pore diameter. Thus, at lower temperatures, mesoporosity reservoir provides greater capacity for capillary condensation and, therefore, better humidity regulation functionality. This mesoporosity volume is clearly associated to the transition (non-crystalline) alumina occurring from gibbsite breakdown [23].

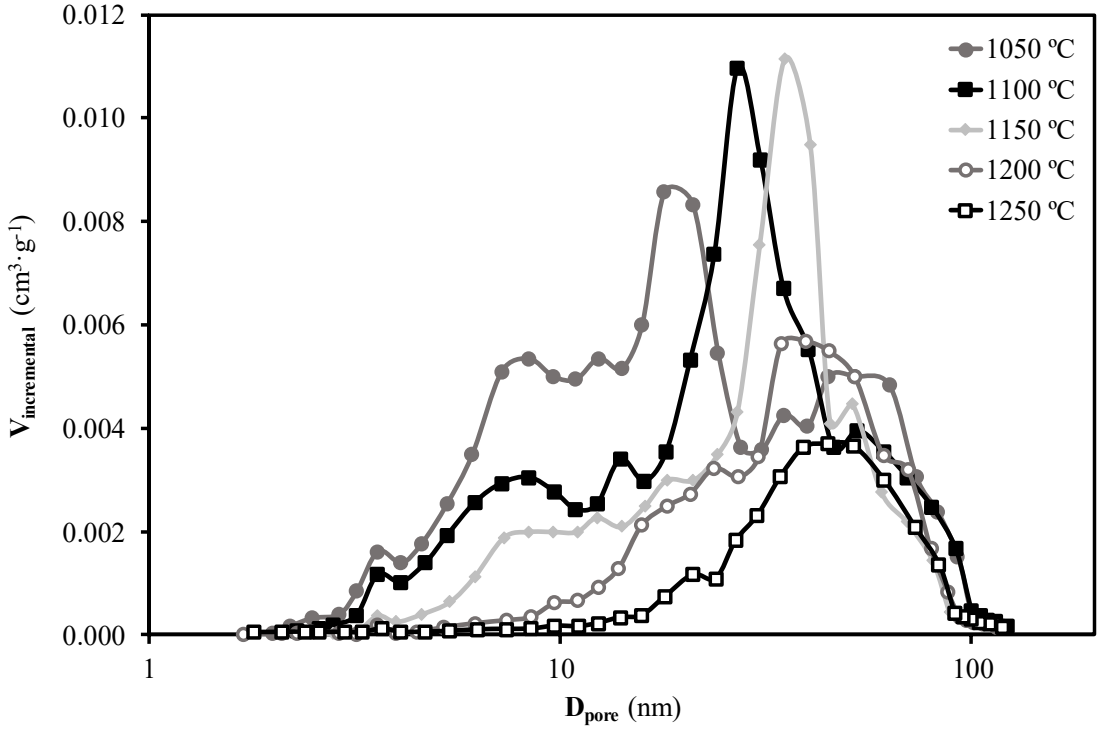

Figure 8. Pore diameter distributions for nitrogen adsorption by BJH method for all samples

Table 5. Specific surface area (S_{BET}), total pore volume accumulated in desorption (V_p) and mean pore diameter (D_p) obtained by nitrogen adsorption for all samples

T (ºC)	S_{BET} ($m^2 \cdot g^{-1}$)	V_p ($cm^3 \cdot g^{-1}$)	D_p (nm)
1050	25 ± 1	0.108 ± 0.006	13 ± 2
1100	19 ± 1	0.097 ± 0.006	16 ± 2
1150	12 ± 1	0.075 ± 0.005	21 ± 2
1200	7.1 ± 0.5	0.056 ± 0.005	27 ± 3
1250	4.3 ± 0.5	0.032 ± 0.005	30 ± 3

3.4 Relation between kinetic parameters and porous microstructure

In order to assess the physical meaning of kinetic model parameters, Figure 9 shows the representation of the equilibrium moisture content of the model (q_e) versus the specific surface area obtained by BET method (S_{BET}). From the analysis of the figure, it can be appreciated a linear correlation between the equilibrium moisture content and the specific surface area for both adsorption and desorption phenomena. This correlation is based on

the much higher contribution of small pores (mesopores) to the porous structure surface when compared with larger pores. The results agree with literature data relating moisture adsorption or isotherms model parameters to mesopore volume and specific surface area [10,33].

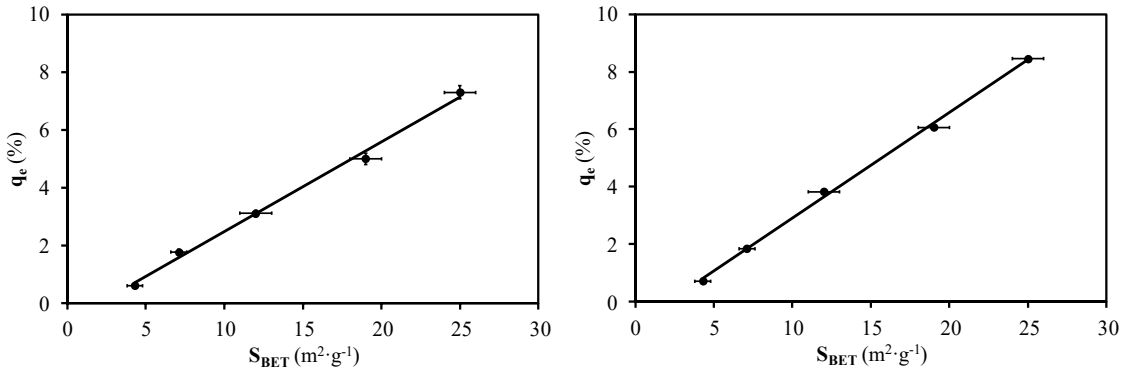

Figure 9. Linear relationship between equilibrium moisture content and specific surface area for a) adsorption for 80 h and b) desorption for 24 h

On the other hand, the sorption rate constant K does not depend so much on the amount of mesopores as on the accessibility of vapour, which is related to the permeability of porous structure. According to literature about models of water permeability in ceramic materials (membranes), there is an approximately linear relationship between the permeability and the product of porosity (P) with square of mean pore diameter (d_{50}) which is consistent with Hagen-Poiseuille equation [34,35]. Figure 10 shows the result of plotting the rate constant of the proposed kinetic model versus the product of the indicated porosity parameters (P and d_{50}) determined from the mercury porosimetry (Table 4). Figure 10 reveals the goodness of the linear fit, so that the correlation between the sorption rate and the permeability for accessibility of water vapour through the interior of the material is confirmed. Despite the differences in rate between adsorption and desorption, the linear fit is adequate for both processes.

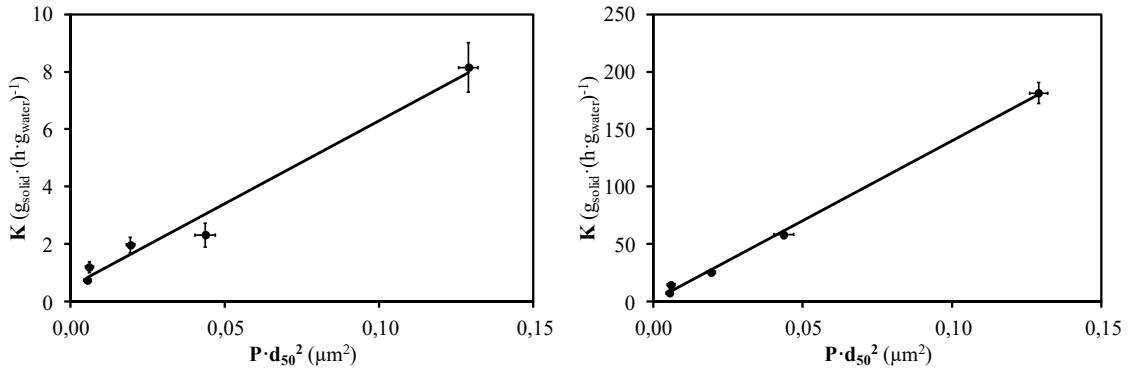

a) b)

Figure 10. Linear relationship between sorption rate constant and porosity parameter ($P \cdot d_{50}^2$) for a) adsorption for 80 h and b) desorption for 24 h

4 Conclusions

The effect of firing temperature on the humidity regulating capacity of a previously studied ceramic tile composition has been addressed. It has been observed that the moisture adsorption and desorption kinetics of the samples fired at five different sintering temperatures follow a pseudo-second order model. Firing temperature greatly affects the humidity regulating capacity, with equilibrium moisture linearly decreasing as temperature increases. This variation corresponds to the microstructural changes that the mineral gibbsite, main component of the starting composition, undergoes with increasing temperature. Thus, the high specific surface area of transition alumina is responsible for the moisture regulating capacity by providing a reservoir of mesopores. However, this microstructure collapses with the sintering process, therefore the moisture regulating capacity practically disappears at temperatures above 1200 ºC, where the crystallisation of the alpha-alumina phase is evident.

It has been found that the equilibrium moisture of the kinetic model is proportional to the specific surface area of the samples, because of the fact that the smaller pores (mesopores), which are responsible for the adsorption-desorption capacity, are in turn those that contribute most to the internal surface area of the porous structure of the samples. As for the other kinetic parameter K, related to the adsorption (or desorption) rate, it has been found that it depends on the permeability or accessibility of water vapour

through the interior of the porous microstructure, which is characterised by porosity and pore size.

Acknowledgments

Acknowledging Ministerio de Ciencia e Innovación of Spanish Government and European Regional Development Fund (ERDF) of European Union for the funding received in the framework of RTC-2017-5904-5 CONFORTMA project.

References

[1] S.B. Sadineni, S. Madala, R.F. Boehm, Passive building energy savings: a review of building envelope components, Renew. Sustain. Energy Rev. 15 (2011) 3617–3631. doi:10.1016/J.RSER.2011.07.014.

[2] R. Pacheco, J. Ordóñez, G. Martínez, Energy efficient design of building: a review, Renew. Sustain. Energy Rev. 16 (2012) 3559–3573. doi:10.1016/J.RSER.2012.03.045.

[3] S. Mirrahimi, M.F. Mohamed, L.C. Haw, N.L.N. Ibrahim, W.F.M. Yusoff, A. Aflaki, The effect of building envelope on the thermal comfort and energy saving for high-rise buildings in hot–humid climate, Renew. Sustain. Energy Rev. 53 (2016) 1508–1519. doi:10.1016/J.RSER.2015.09.055.

[4] E.H. Ishida, Soil-ceramics (earth), self-adjustment of humidity and temperature, Encycl. Smart Mater. (2002). doi:10.1002/0471216275.ESM077.

[5] W. Tian, A. Shui, S. Ke, L. Huang, X. Xi, C. He, W. Chen, B. Du, Low-temperature preparation of humidity self-regulating porous ceramics with high strength performance, Mater. Lett. 243 (2019) 128–131. doi:10.1016/J.MATLET.2019.02.019.

[6] F. Rouquerol, J. Rouquerol, K. Sing, Adsorption by powders and porous solids: principles, methodology and applications, Academic Press, 1999. doi:10.1016/b978-0-12-598920-6.x5000-3.

[7] H. Lan, Z. Jing, J. Li, J. Miao, Y. Chen, Influence of pore dimensions of materials on humidity self-regulating performances, Mater. Lett. 204 (2017) 23–26. doi:10.1016/j.matlet.2017.05.095.

[8] J.L. Amorós, M.J. Orts, S. Mestre, J. Garcia-Ten, C. Feliu, Porous single-fired wall

tile bodies: influence of quartz particle size on tile properties, J. Eur. Ceram. Soc. 30 (2010) 17–28. doi:10.1016/J.JEURCERAMSOC.2009.08.001.

[9] M.J. Lee, H.J. Lee, K. Kim, H.J. Hwang, Fabrication of humidity control ceramics from drinking-water treatment sludge and Onggi soil, J. Korean Ceram. Soc. 53 (2016) 362–366. doi:10.4191/kcers.2016.53.3.362.

[10] O. Watanabe, H. Fukumizu, E.H. Ishida, Development of an autonomous humidity controlling building material by using mesopores, Qualicer. (2008) 19–29.

[11] D.H. Vu, K.S. Wang, B.X. Nam, B.H. Bac, T.C. Chu, Preparation of humidity-controlling porous ceramics from volcanic ash and waste glass, Ceram. Int. 37 (2011) 2845–2853. doi:10.1016/J.CERAMINT.2011.04.118.

[12] P. Du, P. Yuan, D. Liu, S. Wang, H. Song, H. Guo, Calcination-induced changes in structure, morphology, and porosity of allophane, Appl. Clay Sci. 158 (2018) 211–218. doi:10.1016/J.CLAY.2018.03.035.

[13] S.M.B. Respati, R. Soenoko, Y.S. Irawan, W. Suprapto, Effect of low temperature sintering on the porosity and microstructure of porous zeolite ceramic, Appl. Mech. Mater. 836 (2016) 219–223. doi:10.4028/WWW.SCIENTIFIC.NET/AMM.836.219.

[14] L. Tian, L. Wang, K. Wang, Y. Zhang, J. Liang, The preparation and properties of porous sepiolite ceramics, Sci. Rep. 9 (2019) 1–9. doi:10.1038/s41598-019-43918-9.

[15] F. Akhtar, Y. Rehman, L. Bergström, A study of the sintering of diatomaceous earth to produce porous ceramic monoliths with bimodal porosity and high strength, Powder Technol. 201 (2010) 253–257. doi:10.1016/j.powtec.2010.04.004.

[16] M.P. Gómez-Tena, M.A. Bengochea, E. Sánchez, L. Guaita, C. Machí, Development of ceramic formulations with humidity-regulating capability for environmental comfort, Qualicer. (2012) 1–14.

[17] D.H. Vu, K.S. Wang, B.H. Bac, B.X. Nam, Humidity control materials prepared from diatomite and volcanic ash, Constr. Build. Mater. 38 (2013) 1066–1072. doi:10.1016/j.conbuildmat.2012.09.040.

[18] J. Castellano, V. Sanz, E. Cañas, E. Sánchez, Assessment of humidity self-regulation functionality for ceramic tiles, J. Eur. Ceram. Soc. 42 (2022) 716–723.

doi:10.1016/J.JEURCERAMSOC.2021.10.025.

[19] A. Mora, D. Gutiérrez-Campos, C. Lavelle, R.M. Rodríguez, Evaluation of Bayer process gibbsite reactivity in magnesium aluminate spinel formation, Mater. Sci. Eng. A. 454–455 (2007) 139–143. doi:10.1016/J.MSEA.2006.12.004.

[20] D. Njoya, A. Elimbi, D. Fouejio, M. Hajjaji, Effects of two mixtures of kaolin-talc-bauxite and firing temperatures on the characteristics of cordierite-based ceramics, J. Build. Eng. 8 (2016) 99–106. doi:10.1016/J.JOBE.2016.10.004.

[21] A. Tonejc, M. Stubicar, A.M. Tonejc, K. Kosanović, B. Subotić, I. Smit, Transformation of γ-AlOOH (boehmite) and $Al(OH)_3$ (gibbsite) to α-Al_2O_3 (corundum) induced by high energy ball milling, J. Mater. Sci. Lett. 13 (1994) 519–520. doi:10.1007/BF00540186.

[22] B. Xu, P. Smith, L. De Silva, The Bayer digestion behaviour of transition aluminas formed from roasted gibbsite, Int. J. Miner. Process. 122 (2013) 22–28. doi:10.1016/J.MINPRO.2013.04.003.

[23] S. Lamouri, M. Hamidouche, N. Bouaouadja, H. Belhouchet, V. Garnier, G. Fantozzi, J.F. Trelkat, Control of the γ-alumina to α-alumina phase transformation for an optimized alumina densification, Bol. Soc. Esp. Ceram. Vidr. 56 (2017) 47–54. doi:10.1016/J.BSECV.2016.10.001.

[24] R. Goren, H. Gocmez, C. Ozgur, Synthesis of cordierite powder from talc, diatomite and alumina, Ceram. Int. 32 (2006) 407–409. doi:10.1016/J.CERAMINT.2005.03.016.

[25] H. Maeda, E.H. Ishida, Water vapor adsorption and desorption on materials hydrothermally solidified from clay minerals, J. Am. Ceram. Soc. 92 (2009) 2125–2128. doi:10.1111/j.1551-2916.2009.03137.x.

[26] Z. Hu, S. Zheng, Z. Sun, Y. Chen, Y. Yan, Influence of pore structure on humidity control performance of diatomite, Sci. Technol. Built Environ. 23 (2017) 1305–1313. doi:10.1080/23744731.2017.1317576.

[27] E. Levänen, T. Mäntylä, Effect of sintering temperature on functional properties of alumina membranes, J. Eur. Ceram. Soc. 22 (2002) 613–623. doi:10.1016/S0955-2219(01)00334-X.

[28] R.M. German, Coarsening in sintering: grain shape distribution, grain size distribution, and grain growth kinetics in solid-pore systems, Crit. Rev. Solid State

Mater. Sci. 35 (2010) 263–305. doi:10.1080/10408436.2010.525197.

[29] X. Wei, W. Wang, J. Xiao, L. Zhang, H. Chen, J. Ding, Hierarchically porous aluminosilicates as the water vapor adsorbents for dehumidification, Chem. Eng. J. 228 (2013) 1133–1139. doi:10.1016/J.CEJ.2013.05.062.

[30] M.M. Jordan, M.A. Montero, S. Meseguer, T. Sanfeliu, Influence of firing temperature and mineralogical composition on bending strength and porosity of ceramic tile bodies, Appl. Clay Sci. 42 (2008) 266–271. doi:10.1016/J.CLAY.2008.01.005.

[31] V.G. Lee, T.H. Yeh, Sintering effects on the development of mechanical properties of fired clay ceramics, Mater. Sci. Eng. A. 485 (2008) 5–13. doi:10.1016/J.MSEA.2007.07.068.

[32] F. Rodríguez-Reinoso, J. Rouquerol, K. Unger, K. Sing, Characterization of porous solids III, Elsevier, 1994.

[33] D.H. Vu, K.S. Wang, J.H. Chen, B.X. Nam, B.H. Bac, D. Van Binh, A new model for water adsorption in porous ceramics, J. Porous Mater. 20 (2013) 129–136. doi:10.1007/S10934-012-9581-2/FIGURES/7.

[34] W. Li, W. Xing, N. Xu, Modeling of relationship between water permeability and microstructure parameters of ceramic membranes, Desalination. 192 (2006) 340–345. doi:10.1016/J.DESAL.2005.07.042.

[35] M.M. Lorente-Ayza, E. Sánchez, V. Sanz, S. Mestre, Influence of starch content on the properties of low-cost microfiltration ceramic membranes, Ceram. Int. 41 (2015) 13064–13073. doi:10.1016/J.CERAMINT.2015.07.092.